Title
Asprosin is a centrally acting orexigenic hormone

Journal
Nature Medicine, 23(12)

ISSN
1078-8956

Authors
Duerrschmid, Clemens
He, Yanlin
Wang, Chunmei
et al.

Publication Date
2017-12-01

DOI
10.1038/nm.4432

Peer reviewed

HHS Public Access

Author manuscript

Nat Med. Author manuscript; available in PMC 2018 May 06.

Published in final edited form as:

Nat Med. 2017 December ; 23(12): 1444–1453. doi:10.1038/nm.4432.

Asprosin is a centrally-acting orexigenic hormone

Clemens Duerrschmid[1,†], **Yanlin He**[2,†], **Chunmei Wang**[2,†], **Chia Li**[3,4], **Juan C. Bournat**[1], **Chase Romere**[1], **Pradip K. Saha**[1], **Mark E. Lee**[1], **Kevin J. Phillips**[1], **Mahim Jain**[5], **Peilin Jia**[6], **Zhongming Zhao**[6], **Monica Farias**[2], **Qi Wu**[2], **Dianna M. Milewicz**[7], **V. Reid Sutton**[8], **David D. Moore**[1], **Nancy F. Butte**[2], **Michael J. Krashes**[3,4], **Yong Xu**[1,2,*,‡], and **Atul R. Chopra**[1,8,*,‡]

[1]Department of Molecular and Cellular Biology, Baylor College of Medicine, Houston, TX

[2]USDA/ARS Children's Nutrition Research Center, Department of Pediatrics, Baylor College of Medicine, Houston, TX

[3]Diabetes, Endocrinology, and Obesity Branch, National Institute of Diabetes and Digestive and Kidney Diseases (NIDDK), National Institutes of Health, Bethesda, MD

[4]National Institute on Drug Abuse (NIDA), National Institutes of Health, Baltimore, MD

[5]Kennedy Krieger Institute, Baltimore, MD

[6]Center for Precision Health, School of Biomedical Informatics, The University of Texas Health Science Center at Houston, Houston, TX, USA

[7]Department of Internal Medicine, McGovern Medical School, University of Texas Health Science Center at Houston, Houston, TX

[8]Department of Molecular and Human Genetics, Baylor College of Medicine, Houston, TX

Abstract

Asprosin is a recently discovered fasting-induced hormone that promotes hepatic glucose production. Here, we demonstrate that plasma asprosin crosses the blood-brain-barrier and directly activates orexigenic $AgRP^{+}$ neurons via a cAMP-dependent pathway. This signaling results in inhibition of downstream anorexigenic $POMC^{+}$ neurons in a GABA-dependent manner, resulting in appetite stimulation and a drive to accumulate adiposity and body weight. Genetic deficiency of asprosin in humans results in a syndrome characterized by low appetite and extreme leanness, which is phenocopied by mice carrying similar mutations, and one that can be fully rescued by

*Correspondence: Atul R. Chopra M.D., Ph.D., Department of Molecular and Cellular Biology and Department of Molecular and Human Genetics, Baylor College of Medicine, 1 Baylor Plaza, MS130, Houston, TX 77030, chopra@bcm.edu. Yong Xu, M.D., Ph.D., Children's Nutrition Research Center, Department of Pediatrics and Department of Molecular and Cellular Biology, Baylor College of Medicine, 1100 Bates Street #8070, Houston, TX 77030, yongx@bcm.edu.

†Equally contributing first authors

‡Equally contributing last authors

Author contributions

Conceptualization, A.R.C., Y.X.; Basic Investigation, C.D., Y.H., C.W., C.L., J.C.B., C.R., P.K.S., M.J.K., A.R.C.; Clinical Investigation, V.R.S., N.F.B., A.R.C; Resources, M.E.L., K.J.P., M.J., M.F., Q.W., D.M.M., D.D.M.; ANCOVA, P.J., Z.Z.; Writing, A.R.C.

Disclosures

No competing financial interests exist for any of the authors.

asprosin expression. Further, we found that obese humans and mice display pathologically elevated circulating asprosin concentrations, and neutralization of plasma asprosin using a monoclonal antibody reduces appetite and body weight in obese mice, in addition to improving their glycemic profile. Thus, asprosin, in addition to performing a glucogenic function, is a centrally-acting orexigenic hormone, and one that represents a potential therapeutic target to treat both obesity and diabetes.

Introduction

Given the oft scarcity of food, the ability to survive bouts of starvation is one key driving force of evolution. Mammals respond to fasting by activating an enormous cascade of interconnected processes that are precisely coordinated by an array of hormones. Two such coordinated processes during the early stages of fasting are appetite stimulation and hepatic glucose release into the circulation, which, together, ensure the drive to obtain food, and keep the brain nourished and alert while foraging.

Through study of a rare genetic condition in humans – Neonatal Progeroid syndrome (NPS, also known as Marfan Lipodystrophy syndrome, OMIM: 616914), we recently discovered a ~30 kDa fasting-induced hormone, asprosin, which is highly expressed in adipose tissue, and upon secretion, stimulates hepatic glucose release[1]. Asprosin is the 140 amino acid, C-terminal product of the fibrillin-1 protein (encoded by *FBN1*). Consistent with the necessity for hepatic glucose release during fasting, circulating asprosin rises with fasting and drops with refeeding in an acute manner, displaying circadian rhythmicity in coordination with the nutritional state. Here, we demonstrate that peripheral asprosin crosses the blood-brain-barrier to activate the hypothalamic feeding circuitry, leading to appetite stimulation, and over the long term to maintenance of adiposity. Our results demonstrate coordination between two critical pillars of the mammalian fasted state – appetite stimulation and hepatic glucose release – via the same fasting-induced hormone, asprosin, through spatiotemporally distinct mechanisms occurring at the liver and the hypothalamus.

Results

Individuals with NPS display hypophagia

We previously elucidated the complex molecular genetics of NPS that led us to the protein hormone – asprosin[1]. Individuals with NPS have heterozygous, truncating mutations in the *FBN1* gene[1], display a deficiency in plasma asprosin[1] associated with extreme leanness (Fig. 1)[1,2], reduced subcutaneous adipose mass (Fig. 1)[2] and maintenance of insulin sensitivity despite partial lipodystrophy[1,2]. To better understand the energy balance equation in NPS within the context of the observed leanness, we measured food intake and energy expenditure using two independent methods each. We found that the two individuals examined consumed fewer calories on a daily basis than their age and sex matched peers in the lab as well as the home setting (Table 1). Their hypophagia was matched by subnormal daily energy expenditure when measured using indirect calorimetry (lab setting) or the doubly-labeled water method (home setting) (Table 1).

In addition to 24-hr caloric intake and 24-hr energy expenditure measurements, we determined additional parameters related to energy balance to obtain a comprehensive physiological view of the patients with NPS, and reinforce the conclusion that their energy balance equation is tilted in the favor of low caloric intake (Supplemental Tables 1,2). Based on these results we hypothesized that NPS-associated leanness could at least partially be explained by asprosin deficiency, and that asprosin is necessary for normal levels of appetite in humans.

Modeling NPS in mice and determining their physiology

We recapitulated the genetic architecture of human NPS mutations in mice using the CRISPR/Cas9 system. We introduced a small heterozygous deletion (10 bp) encompassing the exon-65/intron-65 border (Fig. 2a). This deletion resulted in skipping of exon 65 and a frame-shift leading to heterozygous ablation of the asprosin coding region (Fig. 2a), thus creating *Fbn1*$^{NPS/+}$ mice, which harbor an identical molecular event documented in a known individual with NPS[3]. Similar to human NPS, we found asprosin concentrations lower than 50% in these mice despite heterozygosity (Fig. 2b), presumably due to previously postulated dominant-negative mechanism of action[1]. Like humans with NPS[2], *Fbn1*$^{NPS/+}$ mice display extreme leanness compared with sex-matched WT littermates (Fig. 2c), which was confirmed using DEXA scans to be due to reduction in both fat mass and lean mass with no statistically significant change in length (Fig. 2d). The reduction in lean mass is not surprising given the underlying Marfan syndrome, which is associated with a reduction in muscle mass and is part of the NPS phenotype due to mutated fibrillin-1 protein[4]. Plasma leptin concentrations were significantly lower in *Fbn1*$^{NPS/+}$ mice on normal chow as well as on a high-fat diet, consistent with their low fat mass (Supplemental Fig. 1a,b).

We then placed *Fbn1*$^{NPS/+}$ mice and WT littermate controls on a high-fat diet for 3 months and found a widening difference in body weight and fat mass between the two groups (Fig. 2e). On standard chow, the body weight curves of *Fbn1*$^{NPS/+}$ mice are already markedly different at weaning age, culminating in a 10 g weight difference at 10 weeks (Fig. 2f). Putting the mice under severe diabetogenic and obesogenic stress (high-fat diet for 6 months, 60% calories from fat) showed that *Fbn1*$^{NPS/+}$ mice were completely protected from both obesity and diabetes, compared with WT mice (Supplemental Fig. 1c–e). Similar to the human disorder, within the context of thinness, *Fbn1*$^{NPS/+}$ mice displayed hypophagia (Fig. 2g) along with a likely compensatory reduction in energy expenditure (Fig. 2h), mirroring the events in human NPS. Energy expenditure was also analyzed using ANCOVA (Fig. 2i) to avoid confounding effects of preexisting low body weight and lean mass in *Fbn1*$^{NPS/+}$ mice, allowing for adjustment of the covariates[5].

The reduction in energy expenditure displayed by *Fbn1*$^{NPS/+}$ mice normalized completely on a high-fat diet (Supplemental Fig. 1f,g), suggesting that the reduction in energy expenditure on normal chow in the setting of human and rodent NPS is a compensatory means to prevent a daily energy deficit, and when daily energy deficit is not a concern, this physiological adaptation to compensate for it disappears. We then assessed the respiratory exchange ratio of *Fbn1*$^{NPS/+}$ mice and found no significant difference in substrate preference compared with WT mice (Supplemental Fig. 1h). Basic vital signs such as heart rate, blood pressure

and body temperature (Supplemental Fig. 1i–k), as well as the thyroid hormone axis were unaffected (Supplemental Fig. 1l) in *Fbn1*$^{NPS/+}$ mice compared with WT. Additionally, we observed no off-target effects of the CRISPR-Cas9 strategy employed for the generation of *Fbn1*$^{NPS/+}$ mice, at four distinct bioinformatically-predicted susceptible loci (Supplemental Fig. 1m)

AgRP^{+} neurons are a well-studied population of orexigenic neurons located in the arcuate nucleus of the hypothalamus[6–8]. In conjunction with low appetite, we found that AgRP^{+} neuron activity was significantly lower in *Fbn1*$^{NPS/+}$ mice compared with WT littermates, demonstrated by decreased firing frequency and resting membrane potential (Fig. 2j). Remarkably, an overnight fast, which normally results in a marked increase in AgRP^{+} neuron activity, had no impact at all in *Fbn1*$^{NPS/+}$ mice (Fig. 2j), suggesting that asprosin deficiency renders these neurons unable to respond even to other potentially compensatory factors. In line with this observation, we found that ghrelin, a well-known orexigenic hormone, and asprosin, act on a partially overlapping subset of AgRP^{+} neurons (Supplemental Fig. 2a). Additionally, ghrelin displayed a blunted ability to activate AgRP^{+} neurons from *Fbn1*$^{NPS/+}$ mice compared with those from WT mice (Supplemental Fig. 2b).

Asprosin is sufficient to rescue key phenotypes of *Fbn1*$^{NPS/+}$ mice

A single subcutaneous dose of recombinant asprosin was sufficient to completely rescue the hypophagia of *Fbn1*$^{NPS/+}$ mice, demonstrating that NPS-associated hypophagia is due to a deficiency of plasma asprosin and not due to some indirect effect of mutated fibrillin-1 (Fig. 3a). Using a complementary experimental approach, a single intracerebroventricular (ICV) injection of recombinant asprosin in *Fbn1*$^{NPS/+}$ mice largely restored the firing rate of AgRP^{+} neurons and completely restored their resting membrane potential to the levels of WT (Fig. 3b).

As a third level of evidence, mouse NPS-associated decrease in AgRP^{+} neuron membrane potential and firing frequency were completely rescued with simple incubation of intact hypothalamic slices with recombinant asprosin, but not with recombinant GFP (Fig. 3c). These results represent the highest level of evidence that NPS-associated hypophagia and depressed AgRP^{+} neuron activity are due to asprosin deficiency, and that normal plasma asprosin concentrations are necessary to maintain appropriate appetite and AgRP^{+} neuron functioning.

Asprosin crosses the blood-brain-barrier and stimulates appetite in rodents

We assessed asprosin concentrations in rat cerebrospinal fluid (CSF) using an asprosin-specific[1] sandwich ELISA, and found it to be present in CSF at concentrations 4- to 5-fold below those in the plasma (Fig. 4a vs. plasma levels reported in ref. 1). Similar to plasma asprosin, CSF asprosin was induced by overnight fasting (Fig. 4a). To assess whether plasma asprosin could cross the blood-brain-barrier and enter the CSF, we injected rats intravenously with recombinant asprosin and looked for presence of the N-terminal His-tag in the CSF. 1 hr after IV injection we detected a strong His-tag signal in the CSF matched by a 6-fold elevation in CSF asprosin, suggesting entry of plasma asprosin into the CSF (Fig. 4b).

To ascertain whether asprosin stimulates appetite, we administered a single dose of bacterially-expressed or mammalian-expressed recombinant asprosin or GFP subcutaneously to WT mice. Asprosin-injected mice displayed greater food intake over the next 24 hr irrespective of which recombinant asprosin preparation was used, compared with GFP-injected mice (Fig. 4c,d). Of note, mammalian-generated asprosin is about twice the molecular weight of the bacterially-generated asprosin, and, as predicted previously[1], this difference is largely due to glycosylation of the mammalian variety (Supplemental Fig. 3a–b). The plasma half-life of the mammalian-generated asprosin is ~145 minutes (Supplemental Fig. 3c) (compared with ~20 minutes for the bacterially-generated version[1]), with a 60 μg subcutaneous dose producing a 40 nM peak plasma level (Supplemental Fig. 3d). Interestingly, asprosin displayed a latent phase of a few hours prior to exerting its orexigenic effect (Fig. 4c,d), which differentiates asprosin from more acute-acting orexigenic agents such as ghrelin[9]. Consistent with subcutaneous injection, we noted an orexigenic effect of asprosin upon direct introduction into the CSF via ICV injection (Fig. 4e). To understand chronic responses, we treated WT mice with daily subcutaneous doses of recombinant asprosin for 10 days. In addition to the expected hyperphagia (Fig. 4f), we found no statistically significant change in energy expenditure, fecal triglyceride content, or body weight (Fig. 4g, Supplemental Figs. 3e–f), a slight decrease in lean mass (likely due to the stress of daily injections) (Supplemental Fig. 3g), and a significant increase in adiposity (Fig. 4h), demonstrating a tilting of the energy balance equation in favor of increased energy intake. A second 10-day gain-of-function strategy using adenovirus-mediated hepatic human *FBN1* overexpression that results in a ~2-fold elevation in plasma asprosin[1] (Supplemental Fig. 3h), showed a similar hyperphagic response (Fig. 4i), body weight increase (Supplemental Fig. 3i), and no statistically significant change in energy expenditure or lean mass (Fig. 4j, Supplemental Fig. 3j), accompanied by an increase in adiposity on normal chow (Fig. 4k), that was potentiated by putting the animals on a high-fat diet (Fig. 4l).

AgRP$^+$ neurons are essential for asprosin-mediated appetite stimulation

We found that recombinant asprosin acutely induced AgRP$^+$ neuron activation via an increase in firing frequency and an increase in membrane potential, while expectedly, recombinant GFP displayed no activity at all (Fig. 5a). We consistently observed that only about 50% of AgRP$^+$ neurons were asprosin-responsive, suggesting that only a subset contain the components necessary for transducing the asprosin signal (Fig. 5b). In addition, we found that asprosin increased the amplitude but not frequency of the miniature excitatory post-synaptic current (mEPSC) of AgRP$^+$ neurons (Fig. 5c,d). This pattern suggests that asprosin increases the responsiveness of AgRP$^+$ neurons to excitatory inputs likely via cell-autonomous mechanisms, rather than regulating the presynaptic inputs per se. We confirmed this by pharmacologically inhibiting synaptic inputs to the AgRP$^+$ neurons and found no decrease in asprosin-mediated activation (Fig. 5e–g).

To ascertain the necessity for AgRP$^+$ neurons for asprosin-mediated appetite stimulation, we injected asprosin in WT and in mice in which AgRP$^+$ neurons were ablated[8]. AgRP$^+$ neuron ablation completely eliminated asprosin's orexigenic drive on a normal-chow diet (Fig. 5h), demonstrating the *in vivo* necessity of AgRP$^+$ neurons for asprosin-mediated appetite stimulation. Of note, when exposed to a high-fat diet, AgRP$^+$ neuron-ablated mice were still

able to respond to asprosin (Supplemental Fig. 4a), suggesting a highly palatable diet's ability to engage different neuronal populations relative to normal hunger signals[10].

Asprosin activates AgRP$^+$ neurons via a Gα_s-cAMP-PKA axis

We assessed dose-dependency of asprosin action in AgRP$^+$ neurons by exposing intact slices to increasing doses of either bacterially- or mammalian-generated recombinant asprosin. We found a dose-dependent activation of AgRP$^+$ neurons at the levels of firing frequency and membrane potential for both varieties of asprosin (Supplemental Fig. 4b). The EC_{50} values for both sources of asprosin were found to be in the nanomolar to subnanomolar range, showing great sensitivity of action, well within the range in which endogenous asprosin exists in the CSF (Supplemental Fig. 4b).

Asprosin-mediated AgRP$^+$ neuron activation, at the level of both firing frequency and resting membrane potential, could be completely prevented by pre-treating with Suramin (heterotrimeric G-protein inhibitor), NF449 (Gα_s inhibitor), NKY80 (adenylate cyclase inhibitor), and PKI (protein kinase A inhibitor) (Supplemental Fig. 4c). Conversely, pre-treating with PTX (Gα_i inhibitor) or with [D-Lys3]-GHRP-6 (ghrelin receptor inhibitor) had no impact on asprosin's ability to activate AgRP$^+$ neurons (Supplemental Fig. 4c). These results suggest that signaling via G-proteins (specifically Gα_s), adenylate cyclase, cAMP and PKA is necessary for asprosin-mediated AgRP$^+$ neuron activation, while Gα_i and ghrelin receptor are dispensable. The same pattern was observed when looking at the proportion of AgRP$^+$ neurons activated by asprosin (Supplemental Fig. 4d).

Asprosin inhibits anorexigenic POMC$^+$ neurons

POMC$^+$ neurons are an anorexigenic population of neurons within the arcuate nucleus that function coordinately with AgRP$^+$ neurons. We found that asprosin acutely inhibited ~85% of the POMC$^+$ neurons by reducing their resting membrane potential and firing frequency (Supplemental Fig. 5a,b). In addition, asprosin increased the frequency but not amplitude of the miniature inhibitory post-synaptic current (mIPSC) in POMC$^+$ neurons (Supplemental Fig. 5c,d). In contrast to the demonstrated direct action on AgRP$^+$ neurons, asprosin's ability to hyperpolarize POMC$^+$ neurons was dependent on intact GABAergic input, suggesting indirect action via surrounding GABAergic neurons (Supplemental Fig. 5e–g). Blockade of glutamatergic inputs on the other hand, did not affect asprosin-mediated POMC$^+$ neuron hyperpolarization (Supplemental Fig. 5f). Since AgRP$^+$ neurons are a GABAergic neuronal population that projects to POMC$^+$ neurons[11,12], we tested the effects of AgRP$^+$ neuron ablation on asprosin-mediated POMC$^+$ neuron hyperpolarization. AgRP$^+$ neuron ablation completely prevented asprosin-mediated hyperpolarization in POMC$^+$ neurons (Supplemental Fig. 5h). This suggests that AgRP$^+$ neurons are at least one population of upstream GABAergic neurons that transduce asprosin's signal to POMC$^+$ neurons.

We expanded our studies to explore effects of asprosin on other neural populations that are relevant for the regulation of feeding and/or energy expenditure. These include 5-HT$^+$ neurons in the dorsal raphe nuclei (DRN), steroidogenic factor-1 (SF1$^+$) neurons in the ventromedial hypothalamic nucleus (VMH), neurons in the paraventricular nucleus of the hypothalamus (PVH) and dopamine (DA$^+$) neurons in the ventral tegmental area (VTA). As

presented in (Supplemental Fig. 6a), asprosin had no effect on any of the VMH SF1$^+$ neurons and VTA DA$^+$ neurons that we recorded; asprosin only depolarized 7% of DRN 5-HT$^+$ neurons but left the rest 93% unregulated; asprosin depolarized 13% and hyperpolarized 4% of PVH neurons, but left the rest (83%) unregulated. Thus, none of these four neural populations responded to asprosin in a comparable way to AgRP$^+$ neurons.

In contrast, we found that PVH neurons from *Fbn1*$^{NPS/+}$ mice showed significantly elevated firing rate and resting membrane potential (Supplemental Fig. 6b). Importantly, ICV asprosin in *Fbn1*$^{NPS/+}$ mice restored PVH neuron firing activities to the level of WT mice (Supplemental Fig. 6b). Since a direct puff of asprosin did not alter firing activities of the majority of PVH neurons (as demonstrated in Supplemental Fig. 6a), the altered firing activities observed in PVH neurons from *Fbn1*$^{NPS/+}$ mice with or without asprosin likely reflect indirect effects secondary to changes in AgRP$^+$ neuron firing. Since PVH neuron activity can reflect melanocortin tone[13], we tested the impact of asprosin inhibition using immunologic neutralization in the context of chronic Mc4r antagonism (Agouti yellow mice[14] versus WT mice). We found that similar to our previous experiments on WT mice, asprosin neutralization, compared with an irrelevant antibody, significantly reduced food intake in WT mice, despite a different genetic background (KK strain) compared with all our previous studies on C57Bl/6 mice (Supplemental Fig. 6c). In contrast, asprosin neutralization had no impact whatsoever on food intake in age/sex matched Agouti yellow mice (Supplemental Fig. 6c). This result is consistent with the observed stimulatory effects of asprosin on AgRP$^+$ neurons and indicates that asprosin-mediated appetite stimulation requires an intact melanocortin pathway.

An anti-asprosin antibody reduces food intake and body weight in obese mice

Immunologic neutralization of asprosin using a monoclonal antibody resulted in a reduction in AgRP$^+$ neuron firing frequency and membrane potential in normal chow-fed mice (Fig. 6a). This was also observed *in vivo* using Fos protein expression as a marker of AgRP$^+$ neuron activity (Supplemental Fig. 7a,b). This was accompanied by a reduction in daily food intake without an associated change in energy expenditure (Fig. 6b,c). This antibody (Supplemental Fig. 8a) has been previously validated by us for asprosin specificity[1], and we performed detailed epitope mapping for it (Supplemental Fig. 8b). We tested the neutralization activity of this antibody *in vitro* that allowed us to calculate its IC_{50} (Supplemental Fig. 8c), and extended that observation to a calculation of the likely minimum efficacious dose in diabetic mice (Supplemental Fig. 8d). For proof-of-concept *in vivo*, we found a complete lack of neutralization activity in mice treated with streptozotocin (Supplemental Fig. 8e) given that such treatment results in a near absence of circulating asprosin[1]. Importantly, we found that the anti-asprosin antibody completely neutralized asprosin's ability to activate AgRP$^+$ neurons and inhibit POMC$^+$ neurons, while an irrelevant antibody (isotype matched IgG) had no effect (Supplemental Fig. 9a–j), validating the effect of both experimental reagents.

We previously demonstrated that human and mouse (high-fat diet and *Lep*$^{ob/ob}$ mutation for the latter species) obesity is associated with a pathological increase in plasma asprosin[1]. We extended those results to another model of mouse obesity – *Lepr*$^{db/db}$ mutation

(Supplemental Fig. 9k). Similar to previously demonstrated improvements in the glycemic profile of insulin resistant mice[1], we found that asprosin immunologic neutralization reduced daily food intake without affecting energy expenditure in a statistically significant manner in *Lepr*$^{db/db}$ mice (Fig. 6d,e). Daily intraperitoneal dosing over 5 days showed improvement in body weight to go along with the reduced food intake (Fig. 6f). Virtually identical results were obtained using mice on high-fat diet (Fig. 6g–i). These results suggest that chronic asprosin loss-of-function using a pharmacological entity such as a monoclonal antibody produces appetite and body weight reductions, as would be predicted from human and mouse genetic studies of asprosin depletion.

Discussion

Whether circulating asprosin concentration is experimentally decreased (genetic depletion in individuals with NPS, genetic depletion in *Fbn1*$^{NPS/+}$ mice, or acute removal via immunologic neutralization in mice) or increased (adenovirus-mediated overexpression or recombinant protein injection), the result is a corresponding consistent change in appetite and adiposity. Asprosin-mediated AgRP^{+} neuron activation appears to be central to these effects, since AgRP^{+} neuron ablation renders asprosin's orexigenic drive ineffective on a normal chow diet. However, it remains possible that asprosin could also exert its appetite stimulating action via other populations of orexigenic and anorexigenic neurons in addition to AgRP^{+} neurons, as suggested by the ability of AgRP^{+} neuron ablated mice to respond to asprosin when subjected to a high-fat diet.

Similar to what was observed in the liver[1], the Gα_s-cAMP-PKA axis is necessary for asprosin-mediated AgRP neuron activation. This is consistent with the known orexigenic effect of Gα_s and cAMP signaling in AgRP neurons[15], demonstrating a previously unknown circulating factor whose orexigenic activity is centered on this pathway. Furthermore, asprosin inhibits anorexigenic POMC^{+} neurons, which depends on intact GABAergic synaptic input. AgRP^{+} neurons are GABAergic neurons that project to POMC^{+} neurons, and their functional relevance is confirmed by the observation that their ablation largely prevents asprosin-mediated POMC^{+} neuron inhibition.

Individuals with NPS display a significant plasma asprosin deficit along with phenotypic parameters of hypophagia, reduced subcutaneous adipose mass and very low body-mass-indices. Generating a heterozygous *Fbn1*^{NPS} mutation in mice results in a virtual phenocopy of human NPS, with hypophagia, low adipose mass and body weight. The mice also display reduced levels of AgRP^{+} neuron activity. Replenishment of plasma asprosin *in vivo*, via a single subcutaneous injection, completely rescues hypophagia in *Fbn1*$^{NPS/+}$ mice, demonstrating the dependence of NPS-associated hypophagia on plasma asprosin deficiency. Importantly, addition of asprosin *ex vivo* to hypothalamic slices or *in vivo* using an ICV injection largely corrects the depressed firing rate and membrane potential of AgRP^{+} neurons from *Fbn1*$^{NPS/+}$ mice, demonstrating the dependence of AgRP^{+} neurons on asprosin for normal functioning.

Given that asprosin is a circulating hormone, immunologic neutralization using monoclonal antibodies is an attractive pharmacologic loss-of-function strategy for potential therapeutic

applications. We previously demonstrated the efficacy of this strategy against the glucogenic effects of asprosin in insulin-resistant mice, with monoclonal antibody treatment acutely lowering insulin concentrations in high-fat-diet fed and *Lep*$^{ob/ob}$ mice[1]. Here, we found that immunologic asprosin neutralization reduces baseline AgRP^{+} neuron activity and results in a reduction in daily food intake. We extended those findings to obesity by demonstrating that chronic immunologic neutralization of asprosin in two independent mouse models of obesity (diet-induced obesity and *Lepr*$^{db/db}$ mutation) results in a reduction in daily food intake along with a reduction in body weight. Interestingly, the absence of leptin signaling in the setting of the *Lepr*$^{db/db}$ mutation did not affect the result, suggesting distinct mechanisms of action for the two hormones at AgRP^{+} and POMC^{+} neurons. Besides a compensatory decrease in individuals with NPS and *Fbn1*$^{NPS/+}$ mice, no statistically significant effects on energy expenditure were observed in any of the experiments suggesting that the effect of asprosin on the energy balance equation is predominantly on stimulation of appetite. Notably, AgRP^{+} neurons are known to suppress energy expenditure, in addition to their appetite-stimulatory function[7]. However, it is possible that the subset of AgRP^{+} neurons activated by asprosin has a greater impact on appetite than on energy expenditure, compared with the asprosin-unresponsive subset.

FBN1 mRNA is present at much lower levels in the brain relative to other tissues[1], and since we observed crossing of the blood-brain-barrier by plasma asprosin, it is likely that peripherally generated asprosin serves as a central appetite-modulating signal, similar to leptin. Organ-specific ablation of asprosin, particularly in adipose, should help address this and other important questions. Another key question is how asprosin signaling fits in the balance exerted by existing orexigenic and anorexigenic hormones such as ghrelin, leptin and insulin. We demonstrated that asprosin and ghrelin activate a partially overlapping subset of AgRP^{+} neurons; asprosin-deficiency renders AgRP^{+} neurons less responsive to ghrelin-mediated activation; ghrelin receptor is dispensable for asprosin-mediated AgRP^{+} neuron activation; leptin receptor (*Lepr*$^{db/db}$) is dispensable for asprosin loss-of-function induced reduction in food intake and body weight; and previously demonstrated cross-talk with insulin's gluco-modulatory actions at the liver[1]. Additionally, the asprosin cell-surface receptor remains unidentified and is a focus of active work in our laboratory.

Thus, the emerging picture of asprosin is as a glucogenic and orexigenic hormone that originates in adipose and is exquisitely sensitive to the whole-body energetic status, rising with fasting and abating with feeding. It performs two critical fasting-related functions (hepatic glucose production and appetite stimulation) using the same cAMP second messenger system, albeit using distinct spatiotemporal mechanisms at two distinct organs. It is possible that central (neuronal) asprosin action could influence its peripheral (hepatic) actions or vice versa, but this remains to be explored experimentally. Nevertheless, pathologic elevation of asprosin in human insulin resistance and obesity, and the observed efficacy of asprosin immunologic neutralization against insulin resistance[1] and obesity in mice (this study), suggest that pharmacologic asprosin loss-of-function could serve as a potentially unique therapeutic avenue against such diseases.

Online Methods

Study subjects and ethics statement

Informed consent and permission to use photographs and biological materials for research was obtained prior to participation from all subjects under Institutional Review Board-approved protocols at Baylor College of Medicine. Study subjects were assessed and genomic DNA was analyzed by either whole-exome or Sanger sequencing as reported previously[1].

Doubly labeled water method (DLW)

Total energy expenditure (TEE) was measured over a 10 day period using the DLW method[17–19]. After collection of the baseline urine samples, each participant received by mouth, 0.086 g/kg body weight of $^{2}H_2O$ at 99.9 atom % ^{2}H and 1.38 g/kg body weight of $H_2{}^{18}O$ at 10 atom % ^{18}O (Isotec, Miamisburg, OH). Seven postdose urine samples (1 mL) were collected at home on days 1–10. The urine samples were stored frozen prior to analysis by Gas-Isotope-Ratio Mass Spectrometry. For stable hydrogen isotope ratio measurements, 10 μL of urine without further treatment were reduced to hydrogen gas with 200 mg zinc reagent at 500°C for 30 min. The $^{2}H/^{1}H$ isotope ratios of the hydrogen gas were measured with a Finnigan Delta-E gas-isotope-ratio mass spectrometer (Finnigan MAT, San Jose, CA). For stable oxygen isotope ratio measurements, 100 μL of urine was allowed to equilibrate with 300 mbar of CO_2 of known ^{18}O content at 25° C for 10 h using a VG ISOPREP-18 water-CO_2 equilibration system (VG Isogas, Limited, Cheshire, UK). At the end of the equilibration, the $^{18}O/^{16}O$ isotope ratios of the CO_2 were measured with a VG SIRA-12 gas-isotope-ratio mass spectrometer (VG Isogas, Limited, Cheshire, UK).

Human room respiration calorimetry (indirect calorimetry)

Energy expenditure was measured for 24 hr in a large (34 m^3) calorimeter. During the 24 hr calorimetry, subjects adhered to a schedule of physical activity (treadmill walking), feeding and sleeping. Heart rate and physical activity were recorded using Actiheart (CamNtech, Cambridge, UK). TEE, nonprotein energy expenditure (NPEE), respiratory quotient (RQ), and net substrate utilization were calculated from VO_2, VCO_2, and urinary nitrogen excretion. BMR was measured after a 12 hr fast upon awakening for 30 minutes. Sleeping EE was measured for the entire night sleep period, confirmed by heart rate and motion sensors. Activity energy expenditure (AEE) was computed as TEE-BMR-0.1TEE assuming diet-induced thermogenesis to be 10% of TEE. Physical activity level (PAL) was defined as TEE/BMR. Energy cost of walking for one individual was measured while walking at 2.5 and 3.5 mph for 15 minutes on a treadmill (Vision Fitness T9600).

Dietary recall

A multiple-pass 24 hr dietary recall was recorded in person by a registered dietitian using Nutrition Data Systems for Research (NDSR) (Database version 2005, Nutrition Coordinating Center, University of Minnesota, Minneapolis)[20] and food models and household measures/dishware. The 24 hr recall was obtained without prior notice. The multiple-pass 24 hr recall method uses 3 distinct passes to garner information about a

subject's food intake during the preceding 24-h. Water consumption and vitamin mineral supplements were not included in the dietary assessment. The dietary recall was analyzed by NDSR, nutrient intakes were computed and these measures were used to evaluate diet quantity/quality against the standards set by the Dietary Reference Intakes (DRI).

Animals

All mouse experiments were performed under animal protocols approved by the Baylor College of Medicine Institutional Animal Care and Use Committee and adhering to the guidelines of the Guide for the Care and Use of Laboratory Animals 8th edition by the National Research Council of the National Academies. We used 6- to 12-week-old male WT mice for *in vivo* studies. These are abbreviated as WT in the text. *Lepr*$^{db/db}$ obese mice, a/a, and A^{y}/a mice were purchased from Jackson Laboratories. AgRP^{+} neuron-ablated mice were generated by injecting AgRP-DTR mice with diphtheria toxin [50 ng/g, subcutaneous, Sigma Aldrich D0564] (DT) during the first week after birth[8,10], and AgRP-DTR mice with saline injection served as control mice. For AgRP^{+} neuron-ablated mice on high-fat diet (HFD), AgRP-DTR mice and WT mice were injected with diphtheria toxin. *Fbn1*$^{NPS/+}$ mice were generated at the Baylor College of Medicine Mouse Embryonic Stem Cell Core using a Crispr/Cas9 approach and a colony was maintained in house. Crispr/Cas9 mutagenesis was confirmed by running PCR using primers flanking the mutation site, followed by sequencing of the PCR product. In silico prediction of off-target effects was performed using the Cas-OFFinder[21] and no off-target effects within known genes were found. Mice were backcrossed to WT C57Bl/6 mice for 6 generations to minimize possible off-target mutations. Assessment of off-target mutations in 4 independent non-gene-coding regions (using 3 mismatches as a reference) was carried out and no off-target mutagenesis was identified (Fig. S1m). Male, 6–12-weeks old WT and *Fbn1*$^{NPS/+}$ littermates were used for all experiments. Mice were housed 2–5 per cage in a 12 hr light/12 hr dark cycle with ad libitum access to food and water ("normal chow" – LabDiet 5V5R – containing 63.3% calories from carbohydrates, 22 % calories from protein, and 14.7 % calories from fat). For diet-induced obesity studies, mice were placed on an adjusted-calories diet providing 60 % of calories from fat (Envigo Teklad TD.06414) for 12–16 weeks unless otherwise indicated. Mice were exposed to adenoviral transduction (10^{11} virus particles per mouse) via tail vein injections as described previously[1]. To obtain cerebrospinal fluid (CSF) for asprosin analysis, we contracted BioreclamationIVT to inject 8- to 12-week old male rats intravenously with His-tagged recombinant asprosin followed by sacrificing them and obtaining CSF 1 hr after injection. Flash frozen CSF was shipped to us for further analysis. Glucose tolerance tests (GTT) were performed using standard procedures. A 1.5 mg/g glucose bolus was used. Streptozotocin-induced diabetic mice were generated as reported previously[1].

Labeling of neuron populations

Whole-cell patch clamp recordings were performed on identified AgRP^{+} neurons or POMC^{+} neurons in the brain slices containing the arcuate nucleus of the hypothalamus (ARH). In particular, to identify AgRP^{+} neurons, we crossed Rosa26-tdTOMATO allele onto AgRP-Cre mice[12] to generate AgRP-Cre/Rosa26-tdTOMATO mice, which express TOMATO selectively in AgRP/NPY^{+} neurons. In some studies, we crossed NPY-GFP mice[22] with

Fbn1$^{NPS/+}$ mice to generate NPY-GFP mice with or without the NPS mutation, and GFP-labeled neurons in the arcuate nucleus were recorded. To record POMC^{+} neurons, we crossed Rosa26-tdTOMATO allele onto POMC-CreERT2 mice[23] to generate POMC-CreERT2/Rosa26-tdTOMATO mice, which express TOMATO selectively in mature POMC^{+} neurons upon tamoxifen induction (0.2 mg/g, i.p. 6 weeks of age). For some studies, we crossed the AgRP-DTR allele onto POMC-GFP mice, and these mice received DT or saline injections (described above) to generate mice with or without AgRP^{+} neurons ablated. Similarly, we used TPH2-CreERT2/Rosa26-tdTOMATO mice[24] and DAT-CreERT2/Rosa26-tdTOMATO mice[25] (with tamoxifen induction) to label 5-HT^{+} neurons and dopamine (DA^{+}) neurons, respectively. We used SF1-Cre/Rosa26-tdTOMATO mice[26] to label steroidogenic factor-1 (SF1^{+}) neurons in the ventromedial hypothalamic nucleus (VMH).

Electrophysiology

Six- to 12-week old mice were deeply anesthetized with isoflurane and transcardially perfused with a modified ice-cold sucrose-based cutting solution (pH 7.3) containing 10 mM NaCl, 25 mM $NaHCO_3$, 195 mM Sucrose, 5 mM Glucose, 2.5 mM KCl, 1.25 mM NaH_2PO_4, 2 mM Na-Pyruvate, 0.5 mM $CaCl_2$, and 7 mM $MgCl_2$, bubbled continuously with 95% O_2 and 5% CO_2[27]. The mice were then decapitated, and the entire brain was removed and immediately submerged in the cutting solution. Slices (250 μm) were cut with a Microm HM 650V vibratome (Thermo Scientific). Three brain slices containing the arcuate nucleus were obtained for each animal (Bregma −2.06 mm to −1.46 mm; Interaural 1.74 mm to 2.34 mm), and recordings were made at levels throughout this brain region. The slices were recovered for 1 hr at 34 °C and then maintained at room temperature in artificial cerebrospinal fluid (aCSF, pH 7.3) containing 126 mM NaCl, 2.5 mM KCl, 2.4 mM $CaCl_2$, 1.2 mM NaH_2PO_4, 1.2 mM $MgCl_2$, 11.1 mM glucose, and 21.4 mM $NaHCO_3$) saturated with 95% O_2 and 5% CO_2 before recording.

Slices were transferred to a recording chamber and allowed to equilibrate for at least 10 min before recording. The slices were superfused at 34°C in oxygenated aCSF at a flow rate of 1.8–2 ml/min. GFP or TOMATO-labeled neurons in the ARH were visualized using epifluorescence and IR-DIC imaging on an upright microscope (Eclipse FN-1, Nikon) equipped with a moveable stage (MP-285, Sutter Instrument). Patch pipettes with resistances of 3–5 MΩ were filled with intracellular solution (pH 7.3) containing 128 mM K-Gluconate, 10 mM KCl, 10 mM HEPES, 0.1 mM EGTA, 2 mM $MgCl_2$, 0.05 mM Na-GTP and 0.05 mM Mg-ATP. Recordings were made using a MultiClamp 700B amplifier (Axon Instrument), sampled using Digidata 1440A and analyzed offline with pClamp 10.3 software (Axon Instruments). Series resistance was monitored during the recording, and the values were generally <10 MΩ and were not compensated. The liquid junction potential was +12.5 mV, and was corrected after the experiment. Data were excluded if the series resistance increased dramatically during the experiment or without overshoot for action potential. Currents were amplified, filtered at 1 kHz, and digitized at 20 kHz. Current clamp was engaged to test neural firing frequency and resting membrane potential (RM) at the baseline and puff delivered recombinant Asprosin (500 ms at various concentrations indicated in the figures). Depolarization was defined as > 2 mV elevation of the resting membrane potential, while hyperpolarization was defined as > 2 mV reduction of the resting membrane potential,

values between a 2 mV reduction and a 2 mV elevation was defined as irresponsive. For the asprosin antibody pre-incubation experiment, asprosin and anti-asprosin mAB or IgG were gently mixed at a 1:100 ratio, and then kept on ice for 1 hr before recording. After $AgRP^+$ or $POMC^+$ neuron response to asprosin alone was confirmed, the mixture of recombinant asprosin and anti-asprosin mAb or IgG was perfused to treat the $AgRP^+$ or $POMC^+$ neurons for 4 minutes. In some experiments, the aCSF solution also contained 1 μM tetrodotoxin (TTX)[28] and a cocktail of fast synaptic inhibitors, namely bicuculline (50 μM; a GABA receptor antagonist)[29] DAP-5 (30 μM; an NMDA receptor antagonist)[30] and CNQX (30 μM; an NMDA receptor antagonist) to block the majority of presynaptic inputs; in some experiments, DAP-5 (30 μM) and CNQX (30 μM) were included in the aCSF solution to block glutamatergic inputs; in some experiments, bicuculline (50 μM) was included in the aCSF solution to block GABAergic inputs. In some experiments, ghrelin (300 nM, 500 ms puff) was applied to test effects of ghrelin on neural firing frequency and RM. For the miniature excitatory postsynaptic current (mEPSC) recordings, the internal recording solution contained: 125 mM CsCH3SO3; 10 mM CsCl; 5 mM NaCl; 2 mM MgCl2; 1 mM EGTA; 10 mM HEPES; 5 mM (Mg)ATP; 0.3 mM (Na)GTP (pH 7.3 with NaOH). mEPSC in $AgRP^+$ neurons was measured in the voltage clamp mode with a holding potential of −60 mV in the presence of 1 μM TTX and 50 μM bicuculline. mIPSC in POMC neurons was measured in the voltage clamp mode with a holding potential of − 60 mV in the presence of 1 μM TTX and DAP-5 (30 μM; an NMDA receptor antagonist) and CNQX (30 μM; an NMDA receptor antagonist). Frequency and peak amplitude were measured using the Mini Analysis program (Synaptosoft, Inc.). The values for RM, firing frequency, mEPSC and mIPSC were averaged within 2-min bin at the baseline or after asprosin treatment. A neuron was considered depolarized or hyperpolarized if a change in membrane potential was at least 2 mV in amplitude and this response was associated temporally with Asprosin. After recording, slices were fixed with 4 % formalin in PBS at 4°C overnight and then subjected to post hoc identification of the anatomical location of the recorded neuron within the ARH.

Fos immunoreactivity in $AgRP^+$ neurons

NPY-EGFP transgenic male adult mice were injected i.p. with either 250 μl IgG or 250 μl anti-asprosin antibody at 6 PM (the onset of dark cycle), and food was removed. Sixteen hours later, mice were perfused with 10 % formalin. The fixed brains were collected and cut into 25 μm coronal sections (1:5 series). These brain sections were subjected to immunofluorescence staining for Fos, as previously[31]. Briefly, the sections were incubated in primary rabbit anti-Fos antibody (1:1000; catalog #2250, Cell Signaling) overnight, followed by the donkey anti-rabbit AlexaFluor 594 (1:1000; catalog A-21207, Invitrogen) for 1.5 h. Slides were cover-slipped and analyzed using a Leica DM5500 fluorescence microscope with OptiGrid structured illumination configuration. $AgRP/NPY^+$ neurons were visualized as GFP-labelled neurons in the ARH, and the numbers of these $AgRP/NPY^+$ neurons co-labelled Fos immunoreactivity (red fluorescence) were counted. For each mouse, neurons were counted in 10–12 consecutive brain sections containing the ARH, and the average was treated as the data value for that mouse.

Mouse food intake and energy expenditure

Food intake and energy expenditure were measured using the CLAMS System (Comprehensive Lab Animal Monitoring System, Columbus Instruments). Animals were acclimatized in the recording chambers for 48–72 hours, and measurements were taken subsequently for 24 hr during the light cycle and dark cycle. Mice received food and water ad libitum, or after an overnight fast where indicated. Oxygen consumption and food intake were recorded.

As previously described[31], male mice were anesthetized with inhaled isoflurane and stainless steel cannulas (Plastics One) were inserted into the lateral ventricles (0.34 mm caudal and 1 mm lateral from bregma; depth, 2.3 mm). Intracerebroventricular (ICV) cannulation was confirmed by demonstration of increased drinking and grooming behavior within 5 min after administration of angiotensin II (10 ng). These mice received 10 ng GFP (1 μg saline) twice a day for 3 continuous days, and 10 ng asprosin (in 1 μl saline) the last day. The BioDAQ food intake monitoring system (Research Diets, Inc) was used to monitor the food intake of ICV-cannulated mice, and the food intake from the last GFP injection and asprosin were compared.

Energy expenditure was analyzed using ANCOVA in *Fbn1*$^{NPS/+}$ mice and WT littermates to avoid confounding effects of preexisting low body weight and lean mass in *Fbn1*$^{NPS/+}$ mice, allowing for adjustment of the covariates, lean mass or body weight[5].

Mouse body composition

Body composition was analyzed using an ECHO-MRI system (Echo medical systems, Texas) or DEXA scans where indicated. Lean mass, fat mass, and overall body weight were calculated using the manufacturer-provided software.

Recombinant asprosin and GFP

Human *FBN1* (2732–2871 amino acids) cDNA was cloned and subsequently sub-cloned into a pET-22B vector for expression in *Escherichia coli.* The fusion protein that was expressed in *E. coli* is 146 amino acids long, comprised of a six-amino-acid His tag on the N terminus and a 140-amino-acid wild-type asprosin. His-tagged GFP expressed in *E. coli* was used as the control protein. The recombinant proteins were further purified using size exclusion columns and polymyxin B based endotoxin depletion columns (Detoxi-Gel™ Endotoxin Removing Gel by Thermo Scientific Inc.) with as many passages as required to bring the final endotoxin concentration equal to or below 2 EU/ml, and buffer exchanged into a PBS-Glycerol buffer or a 20 mM MOPS, pH 7.0, 300 mM NaCl, 150 mM Imidazole buffer. The purified proteins were subjected to SDS-PAGE analysis to determine the purity level. The His-GFP and His-asprosin proteins used in all recombinant protein experiments were >90% pure with endotoxin concentrations (determined using the Pierce™ LAL Chromogenic Endotoxin Quantitation Kit). Human recombinant asprosin with an IL-2 leader sequence (to aid secretion), an N-terminal 6xHis tag followed by the human asprosin amino acid sequence was produced in mammalian cells by the UNC Protein Expression and Purification Core (UNC at Chapel Hill). Briefly the protein was expressed using the Expi293 transient transfection expression system (Gibco, ThermoFisher) according to manufacturer's

protocols. The media was collected, the cells cleared by centrifugation, and the resulting clarified media was sterile filtered and then concentrated and buffer exchanged into Ni-binding buffer (50 mM $NaPO_4$ pH 7.4, 500 mM NaCl, 25 mM Imidazole) using a tangential flow filtration system (Millipore). Aprosin was purified from this solution via Ni-affinity chromatography followed by size exclusion chromatography using an analytical Superdex75 column (GE Healthcare) equilibrated with PBS with 10% glycerol. The mammalian His-asprosin protein was >90% pure as determined by densitometry (Supplemental Fig. 3i). The source of asprosin (bacterially- or mammalian-expressed) is indicated for each experiment.

Sandwich ELISA and western blot

For the asprosin sandwich ELISA, a mouse anti-asprosin monoclonal antibody against asprosin amino acids 106–134 (human profibrillin amino acids 2838–2865) was used as the capture antibody, and a goat anti-asprosin polyclonal antibody against asprosin amino acids 6–19 (human profibrillin amino acids 2737–2750) from Abnova was used as the detection antibody. An anti-goat secondary antibody linked to HRP was used to generate a signal. For the His-tag sandwich ELISA, the same procedure was used, except for the use of a goat anti-His polyclonal antibody (Abcam) as the detection antibody. EDTA plasma was used for plasma sandwich ELISAs. For the mammalian asprosin western blot, 40 μg mammalian asprosin was enzymatically deglycosylated using a protein deglycosylation mix (New England Biolabs). 20 μg glycosylated mammalian asprosin, 40 μg deglycosylated mammalian asprosin, and 20 μg bacterial asprosin were analyzed for molecular weight comparison.

Characterization of the mouse anti-asprosin monoclonal antibody

An in-vitro assay to test the potential of a mouse IgG monoclonal antibody (mAb) to neutralize asprosin was performed. To evaluate the mAb's neutralization potential, 10 nM asprosin was incubated with varying molar ratios of mAb for 1 hr on ice, and residual asprosin was measured using our sandwich ELISA. The *in vitro* IC_{50} was calculated using GraphPad Prism 6 software, based on either the residual concentration, or absolute extinction values. Using guidelines from the UK NC3Rs (https://www.nc3rs.org.uk/mouse-decision-tree-blood-sampling, retrieved on 2/1/2017) to estimate the blood volume of a 50 g mouse, and setting the mAb molecular weight at 150 kDa, 44 μg mAb per 50 g mouse was determined to be sufficient to neutralize 50 % of endogenous asprosin.

Epitope mapping of the mouse anti-asprosin monoclonal antibody

Eleven octamer peptides with a two-amino-acid overlap covering the known immunization peptide used for developing the mouse anti-asprosin monoclonal antibody – KKKELNQLEDKYDKDYLSGELGDNLKMK – were printed in spots on glass slides by Raybiotech (Raybiotech, Norcross, GA) and incubated with the monoclonal antibody. The antibody was detected using a biotinylated anti-mouse antibody, followed by streptavidin conjugated with a fluorophore. Fluorescence of spots corresponding to specific octamer peptides was recorded. The results were reported in raw fluorescence (arbitrary numbers), where the highest number signifies strongest fluorescence and strongest antibody binding.

Asprosin plasma half-life and peak concentration

Mammalian-expressed Asprosin (UNC) was labeled with biotin using a EZ-Link Sulfo-NHS-Biotin kit (Thermo Scientific), and excess biotin was removed using a Zeba Spin desalting column (Thermo Scientific). Final protein concentration was estimated using a BCA assay (Thermo Scientific). Approximately 60 μg/mouse of labeled asprosin was injected subcutaneously into WT mice. Blood was drawn before injection (baseline), and 30, 60, 120, and 360 min after injection, as well as after 24 and 48 hours. Plasma biotinylated asprosin concentration was determined using a custom designed sandwich ELISA. A plate was coated with the anti-asprosin monoclonal antibody (capture antibody), total plasma asprosin was bound, and only biotinylated asprosin was selectively detected using Streptavidin-HRP. Half-life was calculated using GraphPad Prism 6 software. A 60 μg subcutaneous dose of mammalian asprosin was found to result in a 40 nM peak plasma level 30 min after injection.

Human and mouse adiponectin, leptin, ghrelin, TSH, free T3, free T4

Human adiponectin, mouse adiponectin, human leptin, mouse leptin, human ghrelin (total) and mouse ghrelin (total) ELISA kits (Millipore, Billerica, MA) were used to determine the concentrations of each plasma parameter in flash-frozen, previously unthawed plasma as per the manufacturer's instructions. TSH, free T3, and free T4 were measured using an ELISA kit (Monobind Inc, CA) as per the instructions provided.

Statistics

All results are presented as mean ± SEM. *P* values were calculated by unpaired, two-tailed Student's *t*-test, or by one-way or two-way ANOVA followed by appropriate post-tests. The type of test employed is indicated in the figure legend. For *Fbn1*$^{NPS/+}$ mice, data was additionally analyzed using analysis of covariance (ANCOVA) to account for covariates. For Supplemental Fig 2b, a χ^2 test was employed. Box-plots show whiskers at min and max, the box around the 25^{th}–75^{th} percentile, line at median, dot at mean where appropriate. No data were excluded, except for outliers as determined by the Grubbs' outlier test ($\alpha = 0.05$). Animals were excluded if they were found to be sick or died prematurely (less than 5% of animals). In experiments involving different genotypes, investigators were not blinded. For experiments involving the same genotype, but treatment with rAsprosin, rGFP, anti-asprosin mAb, or IgG, animals were randomly assigned into groups with equal mean and standard error, and data were obtained in a blinded fashion. Food intake, energy expenditure, and body composition measures were performed in a blinded fashion, as long as the genotype was not visually obvious (extreme leanness or difference in fur color). Neuronal experiments were performed in an unblinded manner. For mice a minimum of five mice were used per group. Based on prior experience, we assumed a coefficient of variation of 30%, and with a minimum of five mice we are able to detect a 1.5-fold difference in the means with >80% power and a 1.75-fold difference in the means with 99% power. For the two rat CSF experiments, with an expected difference of >2-fold, a minimum of four rats were used per group. We assumed a coefficient of variation of 30%, and are able to detect a 1.5-fold difference in the means with 65% power and a 1.75-fold difference in the means with 95% power. For electrophysiology experiments, a minimum of 8 neurons are used per group. For

an assumed coefficient of variation of 30% we were able to detect a 1.25-fold difference in the means with 52% power, a 1.5-fold difference with 92% power and a 1.75-fold difference with 100% power. *n* values for each experiment state the number of animals per group, or biological samples from that number of animals, except for electrophysiology experiments: in this setup, the *n* values describe the number of total neurons analyzed per treatment. Symbols in figures correspond to the following significance levels: $*P < 0.05$, $**P < 0.01$, and $***P < 0.001$.

Data availability

Data are available from the authors on reasonable request. A Life Sciences Reporting Summary is available.

Supplementary Material

Refer to Web version on PubMed Central for supplementary material.

Acknowledgments

This work was supported in part by the Baylor College of Medicine Mouse Metabolism Core, funded by the NIH (P30 DK079638), by the Protein and Monoclonal Antibody Production Core, funded by the NIH (P30 CA125123), and by the Mouse Phenotyping Core, funded by the NIH (UM1HG006348). Mammalian Asprosin was provided by the University of North Carolina at Chapel Hill Protein Expression and Purification Core, funded by the NIH (P30 CA016086). C.D. is supported by American Heart Association postdoctoral fellowship (16POST29630010). Y.H. is supported by American Diabetes Association (1-17-PDF-138). C.W. is supported by American Heart Association postdoctoral fellowship (16POST27260254). K.J.P. is supported by the NIDDK (1R01DK111631), the American Diabetes Association (1-17-JDF-009). Z.Z. is supported by the NLM (LM012806). V.R.S. is supported by the NHGRI Baylor-Johns Hopkins Center for Mendelian Genomics (UM1 HG006542). D.D.M. is supported by the R.P. Doherty, Jr. – Welch Chair in Science Q-0022. M.J.K. is supported by the Intramural Research Program of the NIH, and the NIDDK (DK075087). Y.X. is supported by the NIDDK (DK101379) and USDA/CRIS (3092-5-001-059), A.R.C. is supported by the NIDDK (1K08DK102529), the Chao Physician-Scientist Award, the Caroline Wiess Law scholar award, and a departmental laboratory startup package.

References

1. Romere C, et al. Asprosin, a Fasting-Induced Glucogenic Protein Hormone. Cell. 2016; 165:566–579. [PubMed: 27087445]
2. O'Neill B, Simha V, Kotha V, Garg A. Body fat distribution and metabolic variables in patients with neonatal progeroid syndrome. Am J Med GenetA. 2007; 143A:1421–1430.
3. Jacquinet A, et al. Neonatal progeroid variant of Marfan syndrome with congenital lipodystrophy results from mutations at the 3′ end of FBN1 gene. Eur J Med Genet. 2014; 57:230–234. [PubMed: 24613577]
4. Judge DP, Dietz HC. Marfan's syndrome. The Lancet. 2005; 366:1965–1976.
5. Even PC, Nadkarni NA. Indirect calorimetry in laboratory mice and rats: principles, practical considerations, interpretation and perspectives. Am J Physiol Regul Integr Comp Physiol. 2012; 303:R459–76. [PubMed: 22718809]
6. Aponte Y, Atasoy D, Sternson SM. AGRP neurons are sufficient to orchestrate feeding behavior rapidly and without training. Nat Neurosci. 2011; 14:351–355. [PubMed: 21209617]
7. Krashes MJ, et al. Rapid, reversible activation of AgRP neurons drives feeding behavior in mice. J Clin Invest. 2011; 121:1424–1428. [PubMed: 21364278]
8. Luquet S, Perez FA, Hnasko TS, Palmiter RD. NPY/AgRP neurons are essential for feeding in adult mice but can be ablated in neonates. Science. 2005; 310:683–685. [PubMed: 16254186]
9. Nakazato M, et al. A role for ghrelin in the central regulation of feeding. Nature. 2001; 409:194–198. [PubMed: 11196643]

10. Denis RGP, et al. Palatability Can Drive Feeding Independent of AgRP Neurons. Cell Metab. 2015; 22:646–657. [PubMed: 26278050]
11. Atasoy D, Betley JN, Su HH, Sternson SM. Deconstruction of a neural circuit for hunger. Nature. 2012; 488:172–177. [PubMed: 22801496]
12. Tong Q, Ye CP, Jones JE, Elmquist JK, Lowell BB. Synaptic release of GABA by AgRP neurons is required for normal regulation of energy balance. Nat Neurosci. 2008; 11:998–1000. [PubMed: 19160495]
13. Garfield AS, et al. A neural basis for melanocortin-4 receptor-regulated appetite. Nat Neurosci. 2015; 18:863–871. [PubMed: 25915476]
14. Fan W, Boston BA, Kesterson RA, Hruby VJ, Cone RD. Role of melanocortinergic neurons in feeding and the agouti obesity syndrome. Nature. 1997; 385:165–168. [PubMed: 8990120]
15. Nakajima KI, et al. Gs-coupled GPCR signalling in AgRP neurons triggers sustained increase in food intake. Nat Commun. 2016; 7:10268. [PubMed: 26743492]
16. Trumbo P, Schlicker S, Yates AA, Poos M. Food and Nutrition Board of the Institute of Medicine, The National Academies. Dietary reference intakes for energy, carbohydrate, fiber, fat, fatty acids, cholesterol, protein and amino acids. J Am Diet Assoc. 2002; 102:1621–1630. [PubMed: 12449285]
17. Butte NF, Wong WW, Hopkinson JM. Energy requirements of lactating women derived from doubly labeled water and milk energy output. The Journal of nutrition. 2001; 131:53–58. [PubMed: 11208938]
18. Roberts SB. Use of the doubly labeled water method for measurement of energy expenditure, total body water, water intake, and metabolizable energy intake in humans and small animals. Can J Physiol Pharmacol. 1989; 67:1190–1198. [PubMed: 2692794]
19. Schoeller DA. Measurement of energy expenditure in free-living humans by using doubly labeled water. The Journal of nutrition. 1988; 118:1278–1289. [PubMed: 3142975]
20. Johnson RK, Driscoll P, Goran MI. Comparison of multiple-pass 24-hour recall estimates of energy intake with total energy expenditure determined by the doubly labeled water method in young children. Journal of the American Dietetic Association. 1996; 96:1140–1144. [PubMed: 8906138]
21. Bae S, Park J, Kim JS. Cas-OFFinder: a fast and versatile algorithm that searches for potential off-target sites of Cas9 RNA-guided endonucleases. Bioinformatics. 2014; 30:1473–1475. [PubMed: 24463181]
22. Pinto S, et al. Rapid rewiring of arcuate nucleus feeding circuits by leptin. Science. 2004; 304:110–115. [PubMed: 15064421]
23. Berglund ED, et al. Serotonin 2C receptors in pro-opiomelanocortin neurons regulate energy and glucose homeostasis. J Clin Invest. 2013; 123:5061–5070. [PubMed: 24177424]
24. Cao X, et al. Estrogens stimulate serotonin neurons to inhibit binge-like eating in mice. J Clin Invest. 2014; 124:4351–4362. [PubMed: 25157819]
25. Xu P, et al. Activation of Serotonin 2C Receptors in Dopamine Neurons Inhibits Binge-like Eating in Mice. Biological Psychiatry. 2017; 81:737–747. [PubMed: 27516377]
26. Dhillon H, et al. Leptin Directly Activates SF1 Neurons in the VMH, and This Action by Leptin Is Required for Normal Body-Weight Homeostasis. Neuron. 2006; 49:191–203. [PubMed: 16423694]
27. Ren H, et al. FoxO1 Target Gpr17 Activates AgRP Neurons to Regulate Food Intake. Cell. 2012; 149:1314–1326. [PubMed: 22682251]
28. Sohn JW, et al. Melanocortin 4 Receptors Reciprocally Regulate Sympathetic and Parasympathetic Preganglionic Neurons. Cell. 2013; 152:612–619. [PubMed: 23374353]
29. Liu Y, et al. Directed differentiation of forebrain GABA interneurons from human pluripotent stem cells. Nat Protoc. 2013; 8:1670–1679. [PubMed: 23928500]
30. Liu T, et al. Fasting Activation of AgRP Neurons Requires NMDA Receptors and Involves Spinogenesis and Increased Excitatory Tone. Neuron. 2012; 73:511–522. [PubMed: 22325203]
31. Yan C, et al. Apolipoprotein A-IV Inhibits AgRP/NPY Neurons and Activates Pro-Opiomelanocortin Neurons in the Arcuate Nucleus. Neuroendocrinology. 2016; 103:476–488. [PubMed: 26337236]

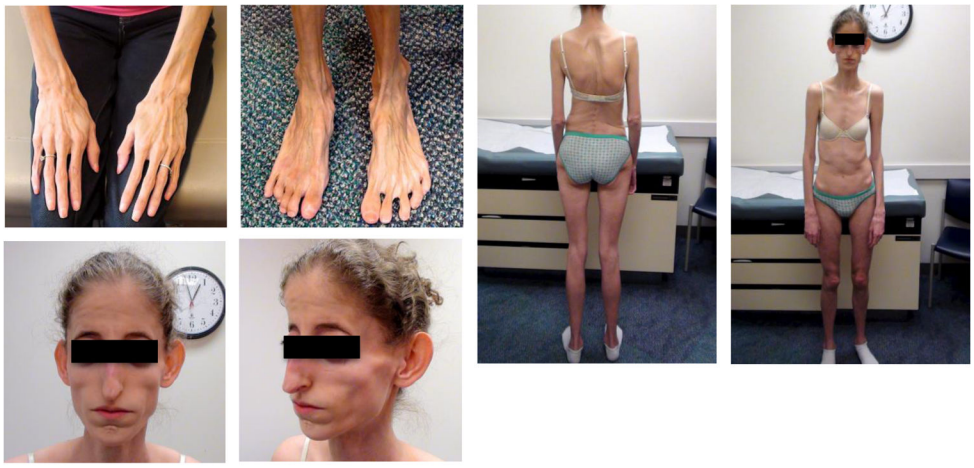

Fig. 1.

Neonatal Progeroid syndrome (NPS) is associated with hypophagia. Representative pictures of two individuals with NPS.

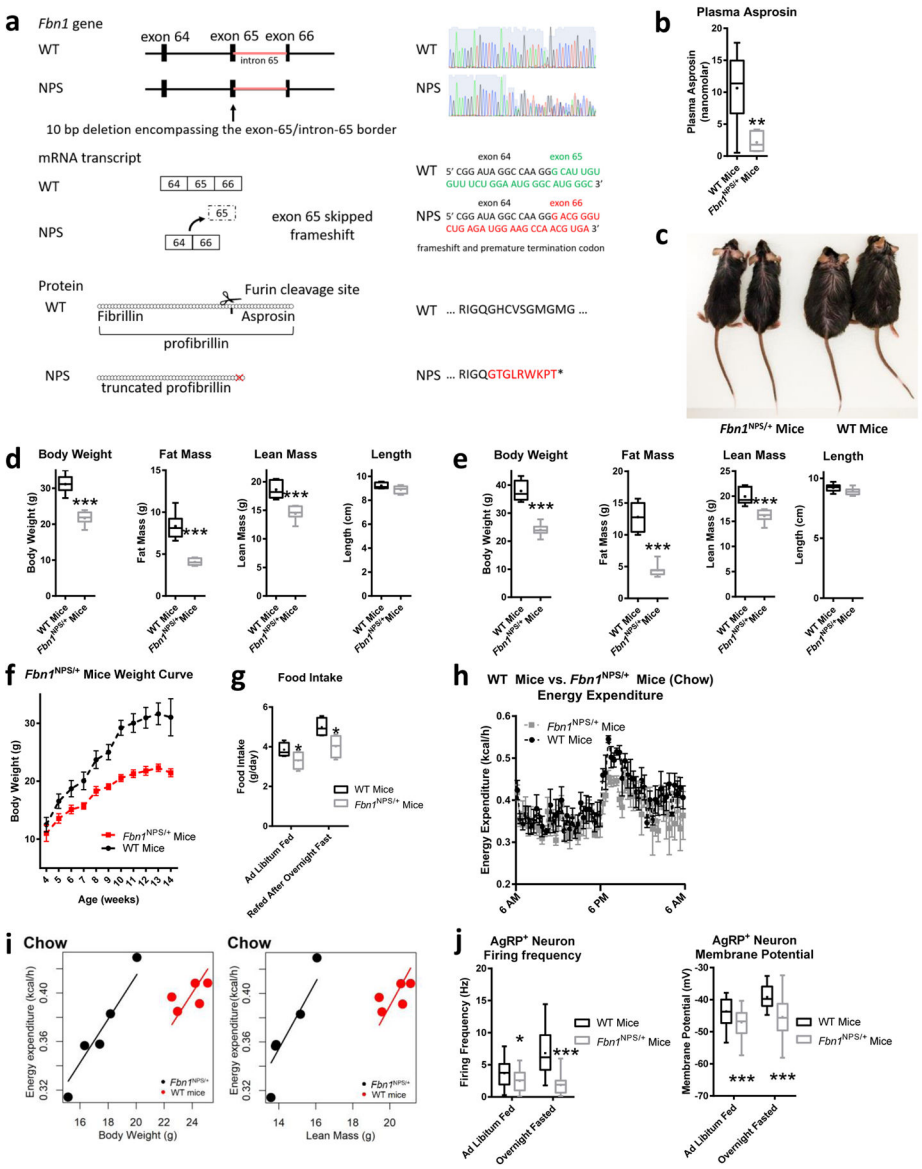

Fig. 2.

Introducing the NPS mutation in mice results in hypophagia, reduced adiposity and protection from diet-induced obesity. (**a**) Schematic depiction of the CRISPR/Cas9 strategy employed to generate *Fbn1*$^{NPS/+}$ mice. A small (10 bp) deletion was introduced at the junction of exon 65 and intron 65 (top left), resulting in loss of a splice site, leading to skipping of exon 65 (middle left) and truncation of profibrillin (bottom left), identical to the molecular events in an individual with NPS[3] (WT and heterozygous mutant sequence trace, WT and mutant mRNA sequence at the deletion site, and resulting WT and mutant protein sequence – top, middle, and bottom right, respectively). (**b**) Sandwich Elisa for endogenous asprosin in plasma of WT and *Fbn1*$^{NPS/+}$ mice (WT $n = 6$, NPS $n = 7$). (**c**) Photograph of a representative set ($n = 12$ for each group) of 5-month-old male WT mice and *Fbn1*$^{NPS/+}$ littermates on a high-fat diet for 3 months. (**d**,**e**) Body composition data using DEXA scans for **d** WT and *Fbn1*$^{NPS/+}$ mice on normal chow (WT $n = 8$, NPS $n = 7$) and e for WT and

Fbn1$^{NPS/+}$ mice on a high-fat diet for 3 months ($n = 8$ per group). (**f**) Weight curves of WT and *Fbn1*$^{NPS/+}$ mice 4 to 14 weeks old ($n = 6$ per group, $P = 0.008$). (**g**) Cumulative food intake over 24 hr in mice from **d** in the ad libitum fed and overnight fasted state using the CLAMs system. (**h**) Energy expenditure was measured over 24 hr mice from **d** using the CLAMs system ($P = 0.16$). (**i**) Analysis of energy expenditure of *Fbn1*$^{NPS/+}$ mice and WT littermates from **d** on normal chow by ANCOVA ($n = 5$ per group, body weight $P = 0.009$, lean mass $P = 0.016$). (**j**) Firing frequency and membrane potential of AgRP^{+} neurons from ad libitum fed and over-night fasted WT and *Fbn1*$^{NPS/+}$ mice (Firing frequency: fed, WT $n = 24$; fed, NPS $n = 23$; fasted, WT $n = 25$; fasted, NPS $n = 20$. Membrane potential: fed, WT $n = 24$; fed, NPS $n = 23$; fasted, WT $n = 25$; fasted, NPS $n = 28$). *$P < 0.05$, **$P < 0.01$, and ***$P < 0.001$. Statistical tests used: two-tailed *t*-test (**b,d,e**) or two-way ANOVA (**f,g,h,j**).

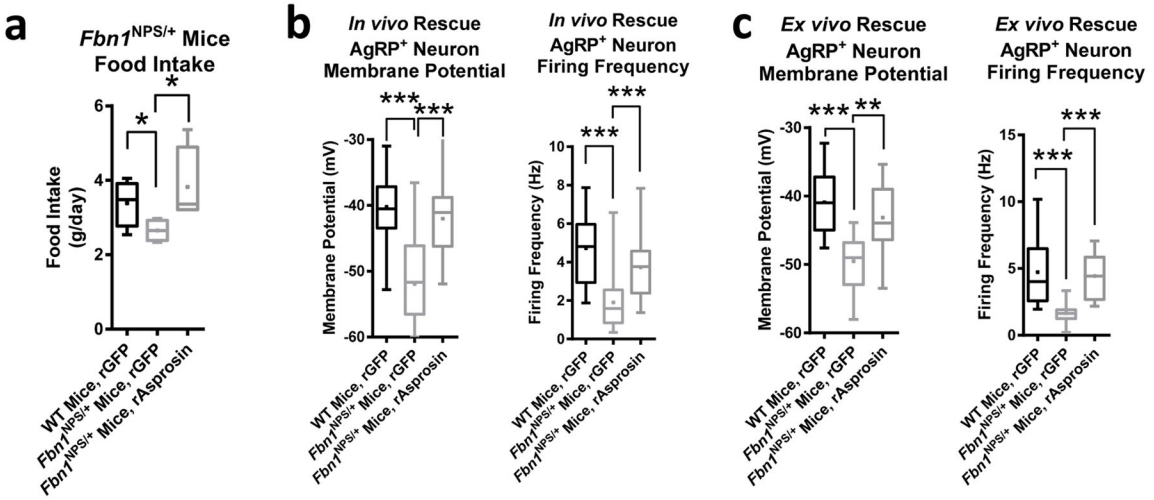

Fig. 3.

Correcting the asprosin deficiency completely rescues hypophagia and depressed AgRP$^+$ neuron activity in *Fbn1*$^{NPS/+}$ mice. (**a**) Cumulative food intake over 24 hr in WT and *Fbn1*$^{NPS/+}$ mice after subcutaneous injection of recombinant GFP or mammalian-expressed recombinant asprosin using the CLAMs system (30 μg/mouse, $n = 5$ per group). (**b**) Membrane potential and firing frequency of AgRP$^+$ neurons from overnight fasted WT and *Fbn1*$^{NPS/+}$ mice 3 hr after ICV injection of recombinant GFP or mammalian-expressed recombinant asprosin as indicated (rAsprosin: 0.5 μg; rGFP: 0.5 μg; membrane potential WT + rGFP: $n = 35$, NPS + rGFP: $n = 31$, NPS + rAsprosin: $n = 20$; firing frequency: WT + rGFP: $n = 25$, NPS + rGFP: $n = 28$, NPS + rAsprosin: $n = 18$). (**c**) Membrane potential and firing frequency of AgRP$^+$ neurons from overnight fasted WT and *Fbn1*$^{NPS/+}$ mice after 2 hr of incubation of intact hypothalamic slices with recombinant GFP or bacterially expressed recombinant asprosin as indicated (rAsprosin: 34 nM; rGFP: 0.5 μg/μL; membrane potential: WT + rGFP: $n = 12$, NPS + rGFP: $n = 14$, NPS + rAsprosin: $n = 14$; firing frequency: WT + rGFP: $n = 12$, NPS + rGFP: $n = 11$, NPS + rAsprosin: $n = 13$). *$P < 0.05$, and ***$P < 0.001$. Statistical tests used: one-way ANOVA (**a–c**).

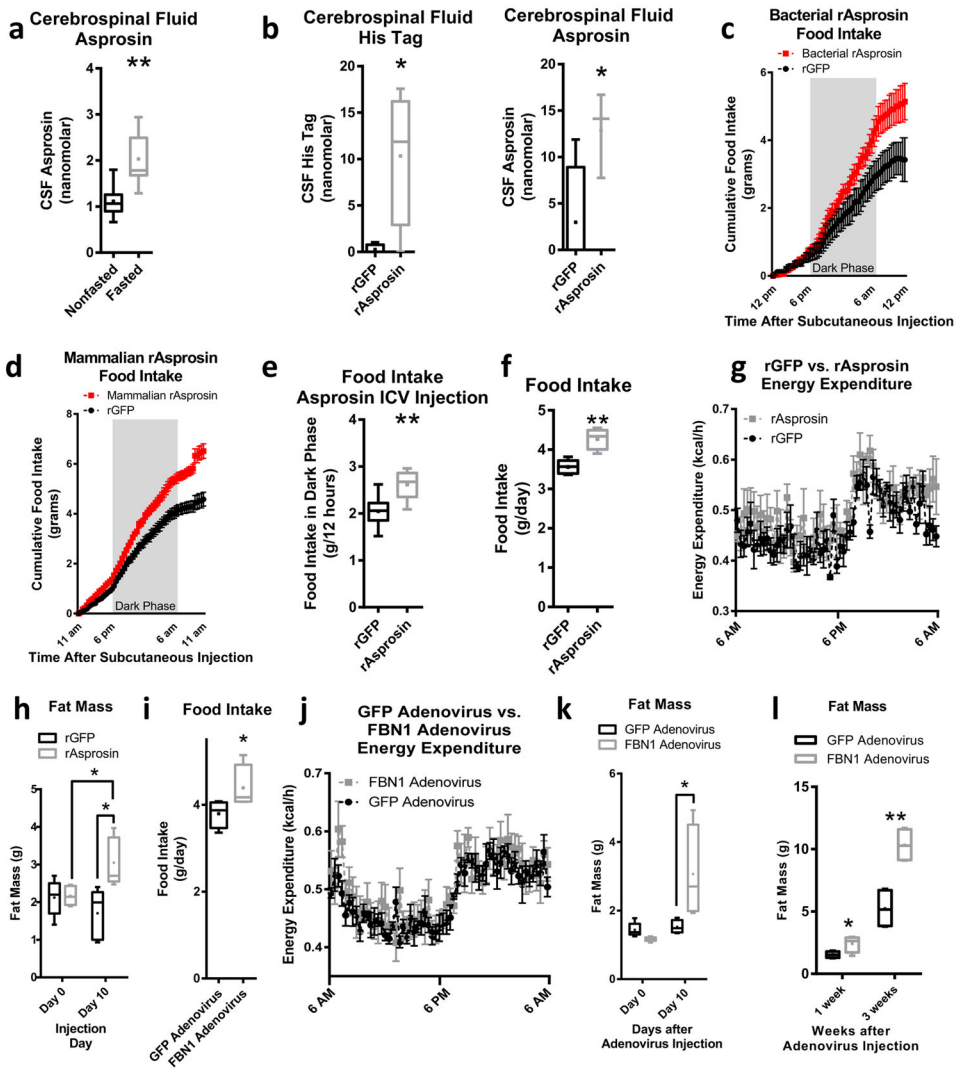

Fig. 4.

Asprosin crosses the blood-brain-barrier and stimulates appetite (**a**) Endogenous asprosin in cerebrospinal fluid of ad libitum fed and over-night fasted rats using a sandwich Elisa ($n = 7$ per group). (**b**) N-terminal His-tag (on bacterially expressed asprosin) and total asprosin (recombinant + endogenous) in cerebrospinal fluid of fasted rats after intravenous injection of bacterially expressed, His-tagged asprosin using a sandwich Elisa (30 μg/mouse, $n = 4$ per group). (**c**) Food intake during 24 hr after a single subcutaneous injection of recombinant GFP or bacterially expressed asprosin in mice using the CLAMs system (30 μg/mouse, $n = 5$ per group, $P = 0.06$). (**d**) Food intake during 24 hr after a single subcutaneous injection of recombinant GFP or mammalian-expressed recombinant asprosin in mice using the CLAMs system (60 μg/mouse, $n = 6$ per group, $P = 0.0003$). (**e**) Cumulative food intake during the dark phase (12 hr) of circadian entrained mice after intracerebroventricular (ICV) injection of recombinant GFP or bacterially expressed recombinant asprosin (rAsprosin: 10 ng; rGFP: 10 ng, $n = 8$ per group). (**f**) Cumulative food intake over 24 hr in mice exposed to 10 days of a single daily injection of recombinant GFP or bacterially expressed asprosin using the

CLAMs system (30 μg/mouse/day, $n = 5$ per group). (**g**) Energy expenditure over 24 hr in mice from **f** using the CLAMs system ($P = 0.15$). (**h**) Fat mass from magnetic resonance imaging (MRI) in mice before and after 10 days of a single daily injection of recombinant GFP or bacterially expressed recombinant asprosin in mice from **f**. (**i**) Cumulative food intake over 24 hr in mice 10 days after adenoviral overexpression of GFP or *FBN1* using the CLAMs system ($n = 5$ per group). (**j**) Energy expenditure over 24 hr in mice from (i) using the CLAMs system ($P = 0.46$). (**k**) Fat mass from MRI in mice from **i** before and 10 days after injection with the GFP or *FBN1* adenovirus ($n = 5$ per group, $P = 0.06$ between *FBN1* group 0 and 10 days). (**l**) Fat mass from MRI in mice 1 week and 3 weeks after injection with the GFP or *FBN1* adenovirus ($n = 5$ per group). *$P < 0.05$, and **$P < 0.01$. Statistical tests used: two-tailed *t*-test (**a,b,e,f,i**) or two-way ANOVA (**c,d,g,h,j,k,l**).

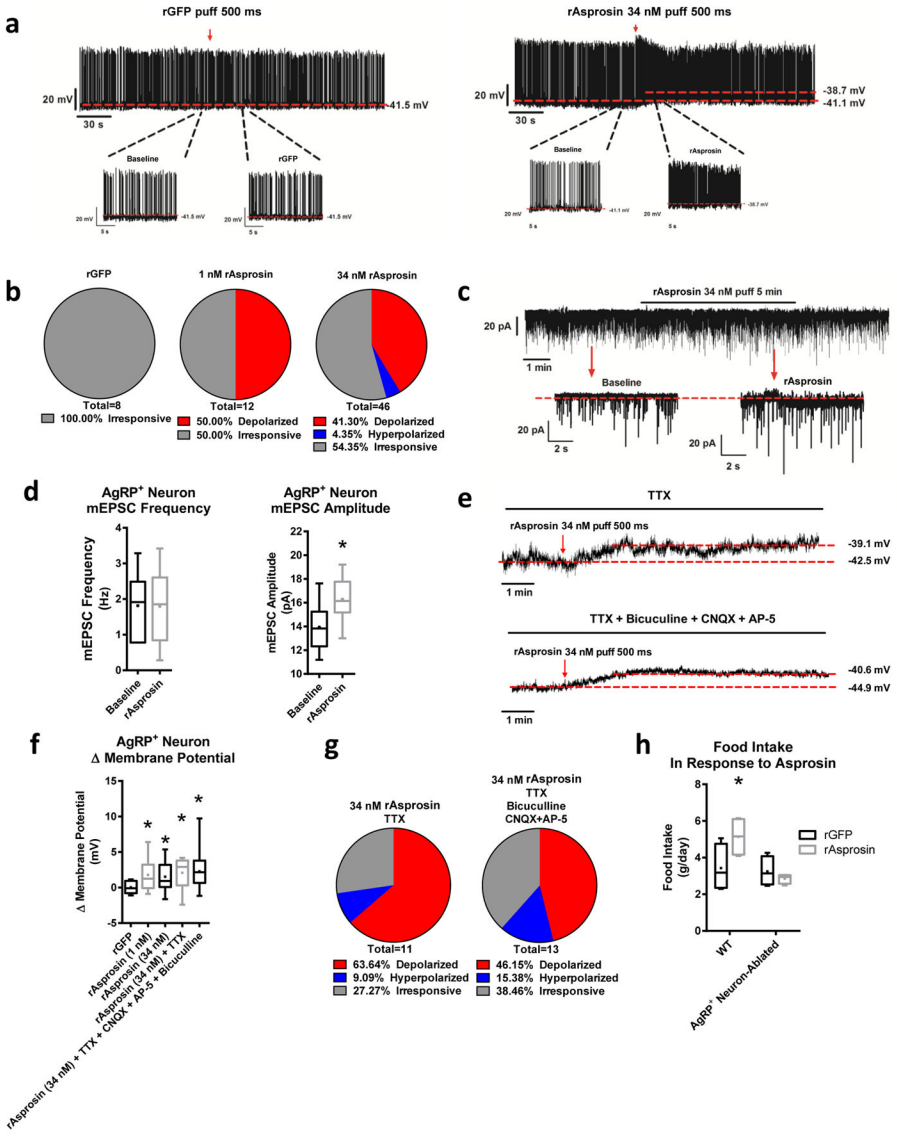

Fig. 5.

AgRP$^+$ neurons are essential for Asprosin-mediated appetite stimulation (**a**) Representative action potential (AP) firing traces of AgRP$^+$ neurons after GFP and bacterially expressed recombinant asprosin treatment. (**b**) Response ratio of AgRP$^+$ neurons after GFP, and 1 nM and 34 nM bacterially expressed asprosin treatment (rGFP $n = 8$, 1 nM rAsprosin $n = 12$, 34 nM rAsprosin $n = 46$). (**c**) Representative traces of miniature excitatory postsynaptic current (mEPSC) in AgRP$^+$ neurons before and after bacterially expressed asprosin treatment. (**d**) mEPSC frequency and amplitude in AgRP$^+$ neurons before and after bacterially expressed asprosin treatment ($n = 6$ per group). (**e**) Representative traces of AgRP$^+$ neuron resting membrane potential in the presence of TTX (1 μM; top), and inhibitor cocktail (AP-5: 30 μM, CNQX:30 μM, bicuculline: 50 μM and TTX 1 μM; bottom). (**f**) Amplitude changes of resting membrane potential in AgRP$^+$ neurons after treatment with GFP, 1 nM and 34 nM bacterially expressed asprosin, or 34 nM bacterially expressed asprosin in the presence of

TTX and inhibitor cocktail (AP-5: 30 μM, CNQX: 30 μM, bicuculline: 50 μM, and TTX 1 μM; rGFP $n = 8$, rAsprosin 1 nM $n = 12$, 34 nM $n = 44$, 34 nM + TTX $n = 11$, 34 nM + TTX + CNQX + AP5 + bicuculline $n = 13$). (**g**) Response ratio of $AgRP^+$ neurons after treatment with bacterially expressed asprosin in the presence of TTX or inhibitor cocktail (AP-5: 30 μM, CNQX: 30 μM, bicuculline: 50 μM, and TTX 1 μM; rAsprosin + TTX $n = 11$, rAsprosin + inhibitors $n = 13$). (**h**) Cumulative food intake on normal-chow in WT and $AgRP^+$ neuron-ablated mice in response to a single dose of GFP or bacterially expressed asprosin (30 μg/mouse, $n = 4$ per group). $^*P < 0.05$. Statistical tests used: two-tailed *t*-test (**e**), one-way ANOVA (**f**), or two-way ANOVA (**h**).

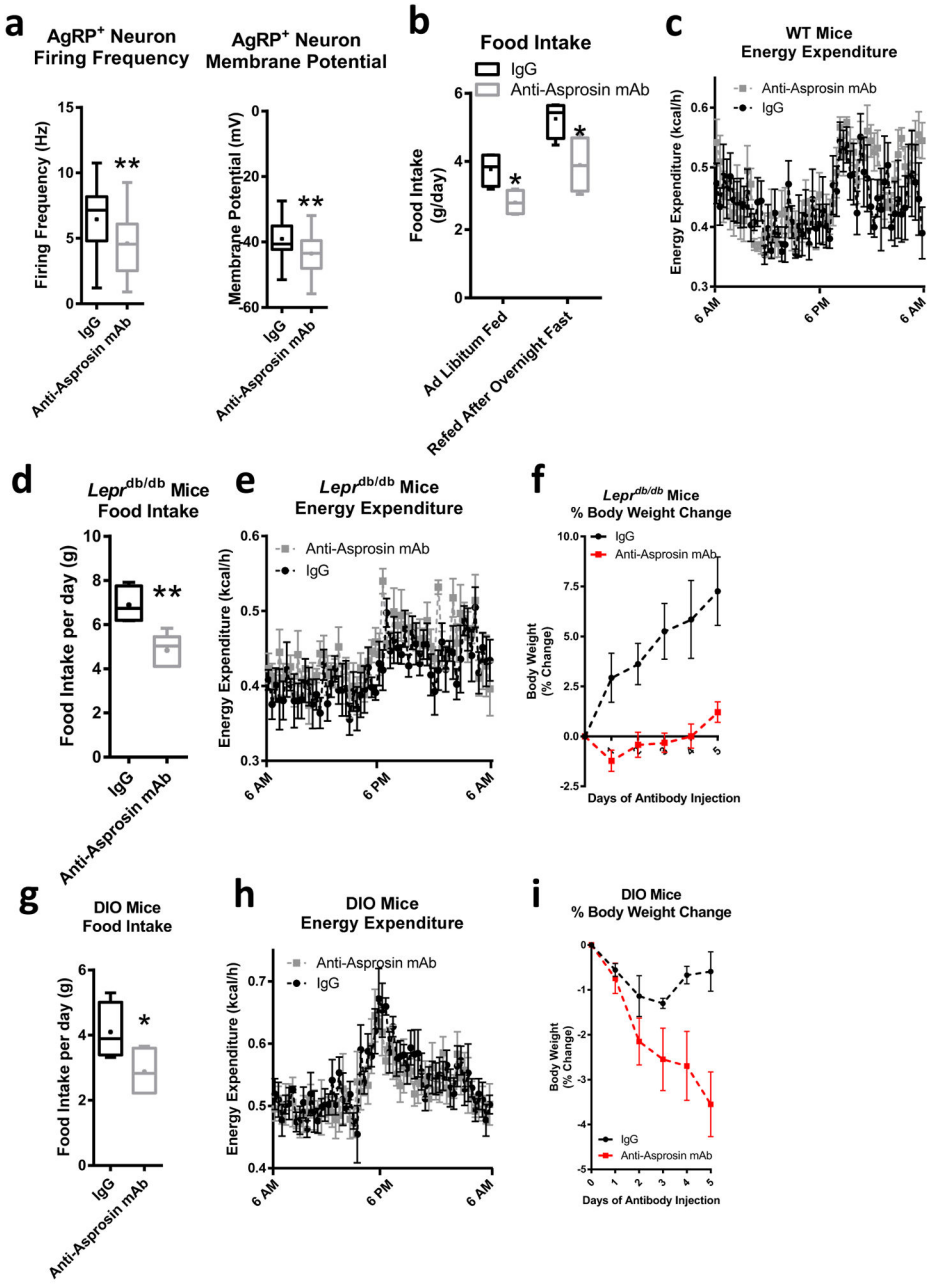

Fig. 6.

Immunologic neutralization of asprosin is protective against obesity (**a**) Firing frequency and membrane potential in AgRP$^+$ neurons from mice 12 hr after IgG control or anti-asprosin monoclonal antibody injection (250 μg/mouse, firing frequency: IgG $n = 27$, anti-asprosin mAb $n = 26$; membrane potential: IgG $n = 33$, anti-asprosin mAb $n = 34$). (**b**) Cumulative food intake over 24 hr in 8-week-old WT mice with one daily injection of IgG control or anti-asprosin mAb in the ad libitum fed and overnight fasted state using the CLAMs system (250 μg/mouse, $n = 5$ per group). (**c**) Energy expenditure over 24 hr in ad libitum fed mice from **b** using the CLAMs system ($P = 0.4$). (**d**) Cumulative food intake over 24 hr in 8-

week-old male *Lepr*$^{db/db}$ mice with one daily injection IgG control or anti-asprosin mAb using the CLAMs system (250 μg/mouse, $n = 5$ per group). (**e**) Energy expenditure over 24 hr in mice from (d) using the CLAMs system ($P = 0.22$). (**f**) Weight change over time in mice from **d** and littermates ($n = 6$ per group, $P = 0.007$). Original weights: 43.8 g for IgG group and 46.9 g for anti-asprosin mAb group. (**g**) Cumulative food intake during 24 hr in 20-week-old male WT mice fed a high-fat diet for 3 months with daily dosing for 5 days of IgG control or anti-asprosin mAb using the CLAMS system (250 μg/mouse, $n = 5$ per group). (**h**) Energy expenditure over 24 hr in mice from **g** using the CLAMs system ($P = 0.67$). (**i**) Weight change over time in mice from **g** and littermates with daily dosing for 5 days with IgG control or anti-asprosin mAb (250 μg/mouse, $n = 6$ per group, $P = 0.05$). Original weights: 50.1 g for IgG group and 50.3 g for anti-asprosin mAb group. *$P < 0.05$, and **$P < 0.01$. Statistical tests used: two-tailed *t*-test (**a,d,g**) or two-way ANOVA (**b,c,e,f,h,i**).

Table 1

Body-mass-indices, reported and measured food intake, and energy expenditure by the doubly labeled water method and indirect calorimetry, in individuals with NPS compared to reference values (in parentheses) for sedentary and active females age 24 and 18 years, respectively[16].

	Patient 1 (NPS, 24 years)	Patient 2 (NPS, 18 years)
BMI [kg/m^2]	9.9 (18.5–24.9)	13 (18.5–24.9)
Food intake - measured [kcal/d]	955 (2000–2400)	1336 (1800–2400)
Food intake – reported [kcal/d]	1087 (2000–2400)	1909 (1800–2400)
Energy expenditure - calorimetry [kcal/d]	1090 (2000–2400)	1759 (1800–2400)
Energy expenditure – DLW [kcal/d]	1339 (2000–2400)	1720 (1800–2400)